Planar Fluorescence Imaging and Three-Dimensional Reconstructions of Capsule RCS Jets

Jennifer A.(Wilkes) Inman[*], Paul M. Danehy[†], David W. Alderfer[‡], and Gregory M. Buck[§]

NASA Langley Research Center, Hampton VA, 23681-2199

and

Andrew McCrea[**]

Alliant Techsystems (ATK), Space Division, Hampton VA, 23681-2199

Planar laser-induced fluorescence (PLIF) flowfield visualization has been used to investigate reaction control system (RCS) jet flows in the wake of hypersonic capsule reentry vehicles. Pitch, roll, and yaw RCS jets were all studied. PLIF was used to obtain off-body flow images at planar slices in these flowfields, which are not easily visualized by other techniques owing to characteristically low gas density. When viewed individually, these slices are shown to provide spatially and temporally resolved information, including the locations and characteristics of turbulent flow structures and the location of the jet flow relative to the vehicle. In addition, ensembles of slices, acquired at multiple locations throughout the flowfield, are combined using computer visualization techniques to

[*] Research Scientist, Advanced Sensing and Optical Measurement Branch, MS 493, AIAA Member

[†] Research Scientist, Advanced Sensing and Optical Measurement Branch, MS 493, AIAA Associate Fellow

[‡] Research Scientist, Advanced Sensing and Optical Measurement Branch, MS 493

[§] Research Scientist, Aerothermodynamics Branch, MS 408A, AIAA Member

[**] Research Engineer, Advanced Sensing and Optical Measurement Branch, MS 493

reconstruct the three-dimensional shape of the flow. Collectively, the off-body flow visualization data set acquired in these tests represents a valuable compliment to surface measurements, especially as a basis for explaining otherwise perplexing discrepancies between such measurements and computational fluid dynamics (CFD) results. The tests described herein were conducted in the 31-Inch Mach 10 Air Tunnel at NASA Langley Research Center.

Nomenclature

ACM = Apollo Crew Module

CEV = Crew Exploration Vehicle

ESP = electronically scanned pressure

N_2 = nitrogen

NO = nitric oxide

OCM = Orion Crew Module

P_a = ambient pressure in tunnel (during *tunnel off* runs)

P_0 = tunnel plenum (aka total or stagnation) pressure

P_j = jet plenum pressure

PLIF = planar laser-induced fluorescence

PSP = pressure-sensitive paint

RCS = reaction control system

TSP = temperature-sensitive paint

UV = ultraviolet

ViDI = Virtual Diagnostics Interface

Introduction

Since the Apollo era of manned spaceflight, capsules have been used as one means of reentry through Earth's atmosphere. The next generation of NASA spacecraft is being designed to include such a reentry capsule, named

the Orion Crew Module (OCM). Whereas the Apollo and *Союз* (Soyuz) reentry capsules were sized to carry three people, the OCM is being designed to carry up to six people.[1] The design requirements of a larger capsule have brought experimental and computational studies of hypersonic capsule flows into the spotlight. One design challenge concerns the reaction control system (RCS) thruster nozzles, and in particular their nozzle geometry and placement. As a result, understanding RCS jet flow and its interaction with the baseline flowfield has become important. Although extensive studies have been conducted on supersonic jets in a cross flow (see, for example, the work by Cassel in Ref. 2 as well as the long list of references therein), the work on RCS jets behind capsules is considerably more scarce.[3,4] Researchers using computational fluid dynamics (CFD) to design RCS jets require both surface and off-body data to validate their codes. Increased surface heating on the vehicle surfaces during RCS jet operation is an important design consideration: such heating can be caused by impingement of the jet on the surface or by interaction between the jet and the gas flowing over the capsule, which can result in flow separations and shock interactions. Another important design consideration is the aerodynamic interaction between the RCS jets and the flow passing over the vehicle. Such interactions can decrease the efficiency of RCS jets. Surface heating and aerodynamic interactions cannot be reliably predicted with CFD. Instead they must be measured in wind tunnel tests to benchmark the computations.

Off-body measurements complement these surface heating and force and moment measurements. Flow visualizations, like those presented in this paper, allow comparisons to be made between computational predictions of the jet flows and measured data. Flow visualization can be compared to CFD to validate the computational prediction of the diameter and length of the jet plume, the trajectory of the jet plume, the location of the Mach disc, the penetration depth of the jet into the oncoming flow – and in the case of multiple jets – the shock interactions between these jets. Furthermore, flow visualization can provide information about transition from laminar to turbulent flow, spatial scales of transitional features in the flow, and length scales of the turbulence. Perhaps the most valuable use of the flow visualization data is to help explain disagreements and discrepancies between predicted and measured heating patterns and force and moment measurements. Flow visualizations provide a detailed, albeit qualitative, understanding of the flow that can help explain the quantitative measurements.

In principle, the schlieren technique could be used to visualize RCS jets. Schlieren has successfully been used by others to visualize RCS jets in supersonic cross flows,[2] which can approximate forebody RCS jets. However in

practice, this method has several limitations in this application involving capsule RCS jets. First of all, capsule RCS jets generally issue into the low-density wake flow and have a low density themselves (as compared to forebody RCS jets), resulting in low contrast schlieren images. In our prior capsule RCS jet investigation, the jets could not be observed with schlieren imaging.[5] Second, the schlieren technique is path-averaged, so three-dimensional information about the jet is lost, including any detailed information about turbulent flow structures. Finally, the shadow of the model itself would obscure much or all of the jet flows, particularly in the case of a roll jet, if schlieren were used. Instead, planar imaging techniques, which visualize planar sections of a flow, are more useful for studying these highly three-dimensional, low-pressure, jet flows. The seeded, nitric oxide planar laser-induced fluorescence (NO PLIF) technique is well suited for this application because it has good signal-to-noise and provides highly spatially resolved images at the low densities of the present experiment.

NO PLIF has previously been used to study numerous supersonic and hypersonic flowfields. NO is naturally present in some facilities and can be readily seeded into others. NO PLIF was used for flow visualization and temperature,[6-9] pressure,[9] mole fraction,[10] and velocity[11] measurements supersonic flowfields. In hypersonic flowfields, NO PLIF was used for flow visualization[12-15] and quantitative measurements.[16-20] More recently, our research group has used NO PLIF to characterize transition and turbulence in hypersonic flows.[21-24] PLIF has been used to study RCS jets in two prior experiments: iodine PLIF was used to study an RCS jet on a flat plate,[25] while our group has used NO PLIF to study a single pitch RCS jet under low flowrate conditions where the jet remained laminar.[5]

In a series of experiments conducted in the 31-Inch Mach 10 Air Tunnel at NASA Langley Research Center in April and May of 2007, both surface and off-body imaging techniques were applied to capsule flows. Pressure-sensitive paint (PSP) and temperature-sensitive paint (TSP) were used to make surface measurements of the effects of RCS jet flow. These results are reported in Ref. 26. Also in this test, planar laser-induced fluorescence (PLIF) of nitric oxide (NO) was used to visualize the off-body flow associated with RCS jets, their interaction with the shear layer bordering the capsule wake flow, and a forebody flow simulating localized ablation. While this paper covers imaging results for all of the RCS jets studied, a more detailed analysis of a subset of the PLIF tests (pitch RCS jets only) is reported in Ref. 27. Details of the design and construction of the model as well as summaries of both the surface and off-body measurements can be found in Ref. 28.

This paper summarizes the first complete qualitative characterization of pitch, roll, and yaw RCS jets of a capsule entry vehicle. The jet operation conditions have much higher flow rates than prior work.[5] This results in turbulent flow in the jet plumes, as well as resulting in jets that are more closely scaled to flight conditions. Additionally, configurations involving multiple RCS jet firings are investigated to characterize the fluid mechanical interaction between these jets.

Experimental Description

A. Nitric Oxide Planar Laser-Induced Fluorescence (NO PLIF) Imaging System

The NO PLIF system consists of the laser system, beam-forming optics and the detection system. The laser system has three main components: a pump laser (Spectra Physics Pro-230-10), a tunable pulsed dye laser (Spectra Physics PDL-2), and a wavelength extender (Spectra Physics WEX). The injection-seeded Nd:YAG laser operates at 10 Hz and pumps the PDL, which contained a mixture of Rhodamine 590 and Rhodamine 610 laser dyes in a methanol solvent. The output of the dye laser and the residual infrared from the Nd:YAG are combined in the WEX, which contains both a doubling and a mixing crystal. The resulting output is tuned to a wavelength of 226.256 nm, chosen to excite the strongly fluorescing spectral lines of the $A^2\Sigma^+ \leftarrow X^2\Pi_\Omega(0,0)$ electronic transition of NO near the Q_1 branch band head. (This transition is often labeled using the simplified notation $A \leftarrow X(0,0)$; consult Refs. 14 and 29 for a more thorough explanation of the spectroscopic notation of nitric oxide).

A monitoring gas cell system is used to ensure that the laser is tuned to the correct spectral line of NO. The gas cell contains a low-pressure mixture of 5% NO in N_2. A quartz window serves as a beam splitter and sends a small portion of the laser energy through windows on either side of the gas cell. A photomultiplier tube (PMT) monitors the fluorescence intensity through a third window at right angles to the path of the laser beam.

The components of this laser system are mounted within a two-level, enclosable, mobile cart. A single monochromatic ultraviolet laser beam exits the cart, creating a relatively safe operating environment. Further details of the system can be found in Ref. 30. For the experiments reported herein, this mobile system was installed adjacent to the NASA Langley Research Center 31-Inch Mach 10 Air Tunnel. A dedicated, adjustable scaffolding with attached mirrors and prisms directed the UV laser beam to the top of the wind tunnel test section. Optics then formed the beam into a ~100 mm (~4 in.) wide by <1 mm (<0.04 in.) thick laser sheet, which was directed vertically

downward through a window in the top of the test section. The section of scaffolding directly above the test section was mounted to a translation stage that could be remotely controlled so that the laser sheet could be swept spanwise through the flowfield during a tunnel run. This was used for alignment of the laser sheet and also for scanning the image plane through the flowfield to visualize three-dimensional flow structures. The resulting fluorescence from NO molecules in the flow was imaged onto a gated, intensified CCD (charge-coupled device) at a viewing angle normal to the laser sheet. This fluorescence occurs via the $A \rightarrow X(0,0\text{-}5)$ transitions, at wavelengths between approximately 226 nm and 285 nm. A 3-mm (0.12-in) thick Schott glass UG-5 filter was placed in front of the camera lens in order to attenuate scattered light at the laser frequency, such that the collected fluorescence ranges in wavelength from approximately 237 nm to 285 nm. This was particularly important when the laser sheet impinged on the model surface or sting, potentially resulting in direct reflections towards the camera. However, use of this 3 mm filter cut down the collected fluorescence intensity by over a factor of 2. Flow visualization images were acquired at 10 Hz with a 1 μs camera gate and a spatial resolution of about 5 pixels/mm (120 pixels/in.).

For this test entry, several improvements have been made to the PLIF system and the data acquisition procedure compared to previous NO PLIF tests in this same facility.[31] The camera was mounted directly to the wind tunnel window, wheras previously, the camera had been mounted on a tripod that rested on the floor. Mounting the camera directly to the tunnel allowed the camera to be placed much closer to the test section, increasing image magnification. This rigid mounting also prevented the camera from being moved accidentally, and thereby losing spatial calibration. Tunnel vibrations caused no observable camera problems. Additionally, a string potentiometer was connected to the translation stage and monitored by the data system so that the laser sheet position could be recorded during the run to facilitate and improve the spatial accuracy of post-processing.

B. Model and Wind Tunnel

A 12.7 cm (5.0 in.) diameter capsule model was fabricated using a steel heatshield, plenum and sting. A stereolithography apparatus (SLA) was used to produce the rest of the test article, including three different capsule afterbodies and numerous RCS jet nozzles. The model was designed with interchangeable parts so that different nozzle and afterbody shapes and configurations could be tested. The design and manufacture of this model is detailed in Buck et al.[28]

For the PLIF experiments, two different afterbodies were tested: an Apollo crew module configuration (labeled ACM-S24), and an Orion crew module configuration (labeled OCM-A24). The model was modified slightly to reduce unwanted laser reflections. A permanent black magic marker was used to color the SLA material matte black. Kapton tape, which absorbs the laser light, was applied to the sting to reduce reflections of the laser from the shiny metal sting. Roughening the Kapton tape using fine-grit sandpaper further decreased reflections.

The 31-Inch Mach 10 Air Tunnel is an electrically-heated blowdown facility located at NASA Langley Research Center in Hampton, Virginia, USA. Reference 32 details this facility, a brief summary of which is provided here. The facility has a nominal Mach number of 10 and a 31-inch square test section and operates on electrically heated, compressed air. Large windows, transparent in the ultraviolet down to approximately 190 nm, form three walls (including top and bottom) of the test section, with the fourth wall formed by the model injection system. The model is side-mounted to this fourth wall. Run durations for the current tests were about one minute. Two different facility stagnation pressures, P_0, were investigated: 2.41±0.02 MPa (350±3 psia) and 8.96±0.03 MPa (1,300±4 psia). The nominal stagnation temperature was 1,005±17 K (1,350±30° F) for the experiments described herein. The two operating pressures simulate freestream unit Reynolds numbers of 1.8E6±0.016E6 m^{-1} (0.56±0.005 million per foot) and 5.9E6± 0.66E6 m^{-1} (1.80±0.02 million per foot), respectively.

Nitric oxide (NO) was seeded into the RCS jet gas using two methods: first, a 5% NO, 95% N_2 gas bottle was used to supply gas directly for some of the test cases (less than 480 kPa / 70 psi jet plenum pressure, P_j). A limitation on supply pressure was caused by the pressure rating of the NO gas cabinet and supply lines. For P_j > 480 kPa (70 psi), a 1 liter mixing chamber was filled with approximately 550 kPa (80 psi) of the 5% NO, 95% N_2 gas mixture and the cell was then pressurized to the desired level with pure N_2. Typical P_j setpoints were 390 kPa (56 psi), 1.7 MPa (250 psi) and 3.4 MPa (500 psi). For many runs, the jet plenum pressure was changed mid-run to allow two test conditions to be investigated in a single tunnel run. During the tunnel runs, the NO-seeded gas flowed through the model and additional N_2 was supplied to the mixing chamber to maintain the desired pressure, if necessary. Consequently, the concentration of NO continually dropped during the runs with an estimated decay half-life of about 15 seconds; thus, over a 60 second run, the NO concentration decreased by more than an order of magnitude. However, the NO PLIF signal intensity did not decrease proportionally because NO self-quenching diminishes as the NO concentration decreases, partially compensating for the loss of NO. The supply pressure was

maintained to within +/- 20% of the desired set pressure by using a conventional single-stage, mechanical pressure regulator attached to a nitrogen bottle. The data system monitored P_j using a Kulite pressure transducer. The data system logged the surface pressure using electronically scanned pressure (ESP) sensors.

A concurrent study involving the same model looked specifically at the effect that the operation of the RCS pitch jet had on the shear layer flow around the vehicle. To briefly summarize, a series of runs were obtained with the wind tunnel not operating. For these *tunnel off* cases, the wind tunnel test section was held at a static pressure chosen to approximately match the measured aft-body pressure during tunnel operation with P_0 = 8.96 MPa (1,300 psi), thus providing a similar pressure ratio across the nozzle for *tunnel off* and *tunnel on* cases. Aft body pressures for the P_0 = 2.41 MPa (350 psi) case were too low for corresponding static-gas tests to be obtained in this facility, and so were not investigated. Data acquired in *tunnel off* mode provide a baseline for comparing the shape and behavior of RCS jets and their interaction with the flow around the model. Additionally, whereas the tests presented in the present paper entailed seeding NO into the RCS jet fluid, NO was instead supplied to a forebody pressure port for a subset of runs to allow visualization of the shear layer nearest the leeward afterbody. Pure N_2 was supplied to the RCS jet and the resulting perturbations to the shear layer flow were imaged. The results of this closely related study may be found in Ref. 27

The normal sequence of operation for tests in the present investigation was to begin NO flow just as the model was injected into the wind tunnel to avoid unnecessary loss of NO from the mixing chamber before the run. The data acquisition was then started and the image acquisition initiated. Consequently, P_j sometimes was not stabilized during image acquisition. An output signal from the intensified CCD indicated to the data acquisition system that the PLIF image acquisition had begun. A remote manual translation stage trigger could be used to start a sweep of the laser sheet across the model for three-dimensional flow visualizations.

Analysis Methods

Single-shot PLIF images (i.e. single-exposure images acquired during a single laser pulse) were processed using background subtraction and image smoothing routines and by applying false color tables. Images were corrected for spatial variations in laser sheet intensity, but neither the laser-sheet intensity nor spatial distribution was measured on a shot-to-shot (i.e. for every laser pulse) basis. Rather, the average laser sheet spatial intensity variation has been

measured by injecting NO into a near vacuum, resulting in uniform NO seeding, prior to the tunnel runs and acquiring an average of 100 PLIF images. Single-shot images were divided by this laser-sheet intensity image. The images were then made into bitmap images or movies for display on the model using ViDI (Virtual Diagnostics Interface) technology as described below. A difficulty encountered in the current experiment was the very large dynamic range in the images, particularly at high jet pressures where fluorescence intensities could range from near camera saturation to the noise level–filling nearly 16 bits of dynamic range. Use of color tables that were suitable for analyzing data obtained in prior experiments resulted in regions of the images showing no fluorescence, even though the raw images display fluorescence when the color table is rescaled. In such situations a common approach is to take the logarithm of the images and then apply the color scale. However when doing this with the current data set much attention was drawn to a blurring or blooming effect near the nozzle exit which was an artifact of the camera, not the flow. So the original linear color mapping scheme was employed, even though it produced images with saturated fluorescence in some locations and no fluorescence and others. Additional details describing the image processing method for smoothing and thresholding the images as well as removing lens and perspective distortion can be found in Ref. 32.

The Virtual Diagnostics Interface (ViDI)[33] is a software tool developed at NASA Langley Research Center that provides unified data handling and interactive three-dimensional display of experimental data and computational predictions. It is a combination of custom-developed software applications and Autodesk® 3ds Max®, a commercially available, CAD-like software package for three-dimensional rendering and animation.[34] ViDI technology can be applied to three main areas: 1) pre-test planning and optimization; 2) visualization and analysis of experimental data and/or computational predictions; and 3) establishment of a central hub to visualize, store and retrieve experimental results. For this experiment, ViDI was used for post-test visualization of the PLIF data as in Ref. 32. Such visualizations are valuable precisely because of the ease with which a consumer of the data can develop a “feel” and intuition for the imaging data as they relate to the overall flowfield in scale, location, and orientation.

The three-dimensional structure of the flow visualized by the PLIF data can be reconstructed in a *pseudo-volume rendering* form in the ViDI software. During several of the wind tunnel runs, the laser light sheet was traversed at a constant velocity through regions of interest. The PLIF images acquired during each traverse of the laser light sheet

were de-warped, scaled to their real-world dimensions, and placed in the proper location with respect to the three-dimensional model of the test configuration within the virtual environment. All portions of the data images that did not contain PLIF signal were made transparent. With all images from a single scan displayed simultaneously, the resulting "stack" of semi-transparent images revealed the boundaries and three-dimensional geometry of the jet flow. Due to the close spacing of the individual data images, this pseudo-volume rendering was similar in appearance to a true volume rendering, in which a three-dimensional jet-flow object would be created from the intensity data contained in the PLIF images.

Results

A. Overview of Test Campaign

A summary of the test parameters covered during these tests is presented in Tables 1 and 2. These tests involved two model afterbodies, the Apollo Crew Module (ACM) and Orion Crew Module (OCM); pitch, yaw, and roll jets; bell- and cone-shaped nozzles; low (2.41 MPa, 350 psi) and high (8.96 MPa, 1,300 psi) tunnel stagnation pressures; low (390 kPa, 56 psi), medium (1.7 MPa, 250 psi), and high (3.4 MPa, 500 psi) jet plenum pressures; three gas-seeding configurations (RCS jet seeding, shear layer visualization, and localized forebody ablation simulation); and two types of PLIF imaging (flow visualization and flow-tagging velocimetry). Table 1 shows a subset of the conditions that were tested using the Apollo capsule aferbody, while Table 2 shows a subset of the conditions for the Orion Crew Module (OCM) afterbody. In Table 2, Yaw (1) and Yaw (4) refer to configurations with either a single nozzle or with four co-located nozzles, respectively.

Apollo Tunnel On, P_0 = 2.41 MPa (350 psi)	Pitch-Bell	Pitch-Cone	Yaw	Roll
390 kPa (56 psi) flow vis.	52, 110**	65, 66	75	82
1.7 MPa (250 psi) flow vis.	53, 54, 55, 110**	65	75	82
3.4 MPa (500 psi) flow vis.	52, 110**	66	73	80, 83

Apollo Tunnel On, P_0 = 8.96 MPa (1300 psi)	Pitch-Bell	Pitch-Cone	Yaw	Roll
390 kPa (56 psi) flow vis.	57, 111**	64, 67, 70*	74	81
1.7 MPa (250 psi) flow vis.	56, 58, 111**	64, 70*	74	81
3.4 MPa (500 psi) flow vis.	57, 111**	67, 70*	72	79

Table 1. Subset of test matrix for Apollo (ACM-S24) model, indicating run numbers. The pressures on the left are the jet plenum pressures, whereas the pressures on the top are the tunnel stagnation pressures.**Runs 110 and 111 were visualized by seeding pure NO out of a forebody pressure port at a low flow rate of 100 sccm while flowing nitrogen out of the RCS pitch nozzle at various pressures (including no flow) and are not shown in this paper. Yaw and roll jets both used bell-shaped nozzles.

	P_0 = 2.41 MPa (350 psi)		P_0 = 8.96 MPa (1,300 psi)	
Orion	Yaw (1)	Yaw (4)	Yaw (1)	Yaw (4)
390 kPa (56 psi) flow vis.	88, 92	98	87, 93	
1.7 MPa (250 psi) flow vis.	92	99	93	100
3.4 MPa (500 psi) flow vis.	88		87	

Table 2. Subset of test matrix for Orion (OCM-A24) model. The pressures on the left are the jet plenum pressures, whereas the pressures on the top are the tunnel stagnation pressures.

B. Interpretation of PLIF Images

The absolute intensity at any given pixel in a PLIF image has a functional dependence on many local flow parameters as given by Eq. 1:[35]

$$S_f = C\,\rho\,\chi_{NO}\,E\,\Phi\left[\sum f_B\,B_{12}\,g_i\right] \tag{1}$$

Here, S_f is the fluorescence signal; C is a constant related to the collection solid angle and the efficiency of the detector; ρ is the local gas density (kg/m^3); χ_{NO} is the local mole fraction of NO; E is the energy in a single laser pulse (J); Φ is the fluorescence yield; f_B is the Boltzmann fraction; B_{12} is the Einstein stimulated absorption coefficient for the probed transition; g_i is the spectral overlap integral; and the sum is over all probed (lower) states. Here, it is assumed that the laser intensity is below the saturation intensity, and that absorption along the path of the laser through the imaged region is negligible. Radiative trapping (whereby an emitted fluorescence photon is reabsorbed by the medium) is neglected. Stimulated emission is also considered to be negligible due to the

relatively small population of the upper state prior to excitation at the temperatures encountered in these experiments.

The fluorescence yield (Φ), Boltzmann fraction ($f_{B,}$) and spectral overlap integral (g_i) are all functions of the local temperature; Φ also depends on the local pressure and mole fractions of each species, while g_i also depends on pressure and the velocity of the gas; the density ρ depends on both temperature and pressure. Since the fluorescence intensity depends on so many local flow parameters, variations in any one of these parameters will affect the resulting intensity in a PLIF image. While this means that the interpretation of PLIF images is not always straightforward, it also means that PLIF images are well suited to detecting fluctuations within a flowfield, and the capability of detecting turbulent structures and fluctuations over a wide range of jet conditions is one of the primary strengths of this work.

As a rough guideline for interpreting PLIF images, the image intensity can be interpreted as concentration of jet fluid. However, this is a vast oversimplification of the physics. Regions of the flow not containing jet fluid have no PLIF intensity. A more thorough interpretation of the PLIF intensity show that it will be higher in regions of lower temperature (due to our choice of a laser frequency which excites transitions having larger Boltzmann fractions at low temperatures); lower pressure (due to the reduced effects of quenching on Φ); higher density (due to the increased number of available fluorescent molecules); and lower mixing (due to the higher mole fraction of nitric oxide and reduced effects of quenching by oxygen, as compared to highly mixed regions of the jet). Conversely, intensity will be lower in high-temperature, high-pressure, low-density, highly-mixed regions of the flow, or parts of the flowfield that have no jet fluid.

Absolute intensity in the images has been arbitrarily adjusted to span the dynamic range of the false color table that has been applied. This false color table has been applied to enhance contrast and to increase sensitivity in regions of low signal. This color table is included in Fig. 1.

As stated above, the imaging resolution of the PLIF images presented herein is approximately 5 pixels/mm (120 pixels/in.) in the imaging plane. Flow structures as small as 4 to 5 pixels in size were routinely observed. The out-of-plane spatial resolution is limited by the finite thickness (~0.5 mm, ~0.02 in.) of the laser sheet. For volumetric data, acquired by translating the laser sheet in the spanwise direction (perpendicular to the imaging plane), the spanwise imaging resolution was determined by the repetition rate of the laser (10 Hz) divided by the rate at which

the laser sheet was translated. Depending on the run, this rate varied from 2.54 mm/s (0.100 in./s) to 4.25 mm/s (0.167 in./s), resulting in spanwise resolutions of 3.9 frames/mm (100 frames/in.) to 2.4 frames/mm (61 frames/in.). The signal to noise ratio (taken to be the average signal intensity divided by the standard deviation of the intensity within a relatively uniform region of the flow) in the brightest parts of the images was typically between about 20 and 30, with the dominant source of noise in these regions being shot noise.

C. Reaction Control System (RCS) Jet Imaging Results

1. Pitch, Yaw, and Roll Jets

For the model configuration with the Apollo backshell, pitch, yaw, and roll RCS jets were studied. Additionally, two different nozzle shapes (bell and cone) were investigated for the pitch jet, whereas yaw and roll nozzles both had a bell-shaped geometry. Reference 27 contains a complete description of the two nozzle shapes. For the model configuration with the Orion backshell, only yaw jets were studied. These yaw jet nozzles had the bell shape. For some Orion runs, a single yaw jet was activated, while for other runs, four closely-spaced yaw jets were activated simultaneously. Results for a selected subset of runs are presented in this section; namely, images are shown for those runs with the high (8.96 MPa, 1,300 psi) tunnel stagnation pressure, P_0, and the medium (1.7 MPa, 250 psi) jet plenum pressure, P_j.

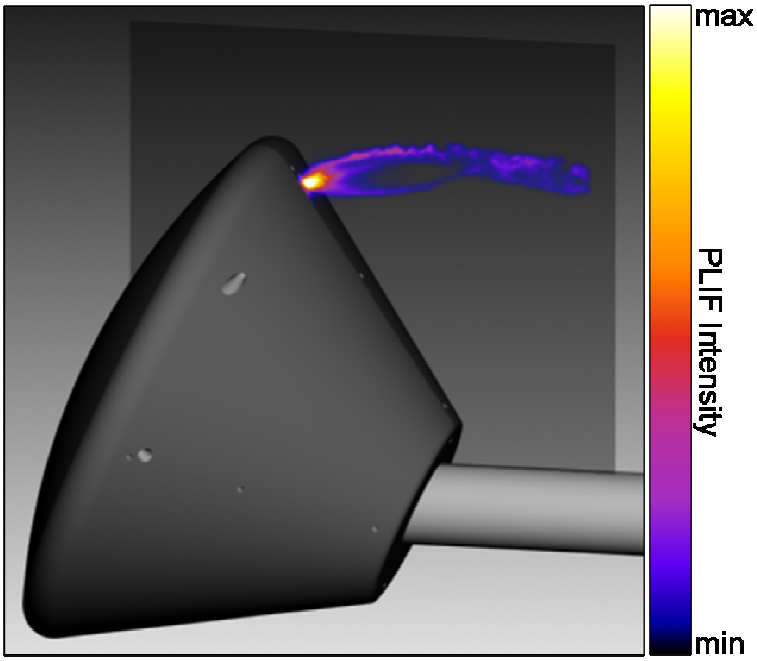

Figure 1. RCS pitch jet. A ViDI (Virtual Diagnostics Interface) rendering showing a single-shot, false-color PLIF image acquired on the centerline of the model. The imaging resolution within the PLIF images is about 4 pixels/mm (102 pixels/in.). Capsule heatshield diameter is 127 mm (5.0 in) and sting diameter is 19 mm (0.75 in.). Run 58, Apollo model (ACM-S24), tunnel stagnation pressure P_0=8.96 MPa (1,300 psi), jet plenum pressure P_j=1.7 MPa (250 psi).

Figure 1 shows a single-shot PLIF image acquired on the centerline of a pitch RCS jet. The flow is effectively frozen during the 1μs gated exposure time of the camera, revealing the instantaneous structure of the jet flow. This allows turbulent flow structures along

the top of the jet to be visualized. Note that the PLIF signal intensity is highest near the nozzle exit where the high density and high mole fraction of NO results in high signal, in spite of the deleterious effects of (relatively) high temperature and high pressure in this same region of the jet. The ViDI rendering includes the Apollo model, showing scale and location of the false-color PLIF image in relation to the model geometry. The six small circular holes seen along the top and side of the capsule are pressure taps used to measure surface pressure on the model. The two larger holes near the junction of the model backshell (afterbody) and heatshield (forebody) are the RCS roll and yaw nozzles. The dark gray square indicates the imaging plane within the field of view of the camera.

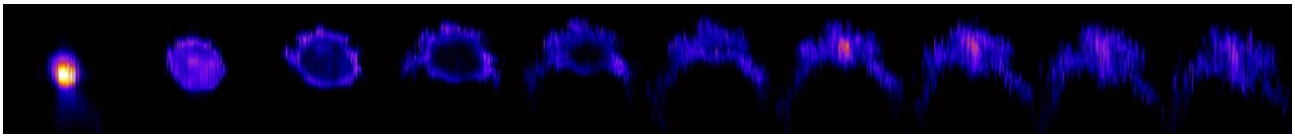

Figure 2. Cross-plane images of RCS pitch jet. Each of these 10 images were reconstructed from 103 single-shot images, acquired during a constant speed spanwise scan of the laser sheet through the jet flowfield. Each measures 25 mm high x 26 mm wide x 0.25 mm thick (in the out-of-plane direction) with a spatial resolution of 4.1 pixels/mm vertically x 3.9 pixels/mm horizontally. They represent planar slices through the flow in planes perpendicular to the centerline image shown in Fig. 1, at evenly-spaced intervals of 7.8 mm (0.31 in.). Run 58, Apollo model (ACM-S24), P_0=8.96 MPa (1,300 psi), P_j=1.7 MPa (250 psi).

One hundred single-shot images were acquired during a spanwise scan of the laser sheet through this jet. A cross-plane view of the RCS jet structure can be reconstructed by extracting PLIF image intensity values at a single streamwise location (e.g. a specific column within each PLIF image) acquired as the laser is swept in the spanwise (crossflow) direction through the RCS jet. This *reslicing* of the image data was performed in the open-source Java-based ImageJ image processing program. Several resliced cross-plane images, shown in Fig. 2, were created at equally-spaced intervals, beginning near the nozzle exit and moving downstream. These images provide views of the jet similar to those that would be seen if the laser sheet were positioned spanwise to the flow and the camera were positioned to view the model from behind. The cross-plane images show a degree of blurring or jaggedness in turbulent portions of the flow because this particular flow has turbulent features and because the single-shot images from which the cross-plane images are constructed are uncorrelated in time. These cross-plane images reveal which flow structures are stable in time and which are time-varying, because the stable flow features lead to smooth features in the resliced images whereas unstable flow features lead to jagged features in the resliced images. The first several slices show a relatively round jet cross section. By the second and third slice, however, periodic azimuthal lobes can be seen developing around the outer upper edge of the jet. These appear to be an azimuthal cosine breakdown mode of transition, previously observed in free jet flows and described in Ref. 22. The two

outermost lobes get progressively larger and become deflected downwards toward the capsule surface. As the jet propagates downstream, the jet core is observed to collapse and the degree of unsteadiness is seen to progressively increase.

In addition to creating cross-plane images, single-shot images from spatial scans of the laser sheet can be used to animate the same data in a movie to show the jet shape at different spatial locations. The single-shot images are placed in relation to their location relative to the wind tunnel model and a series of images are produced, which can either be viewed as a movie or selected frames can be presented as an image montage.

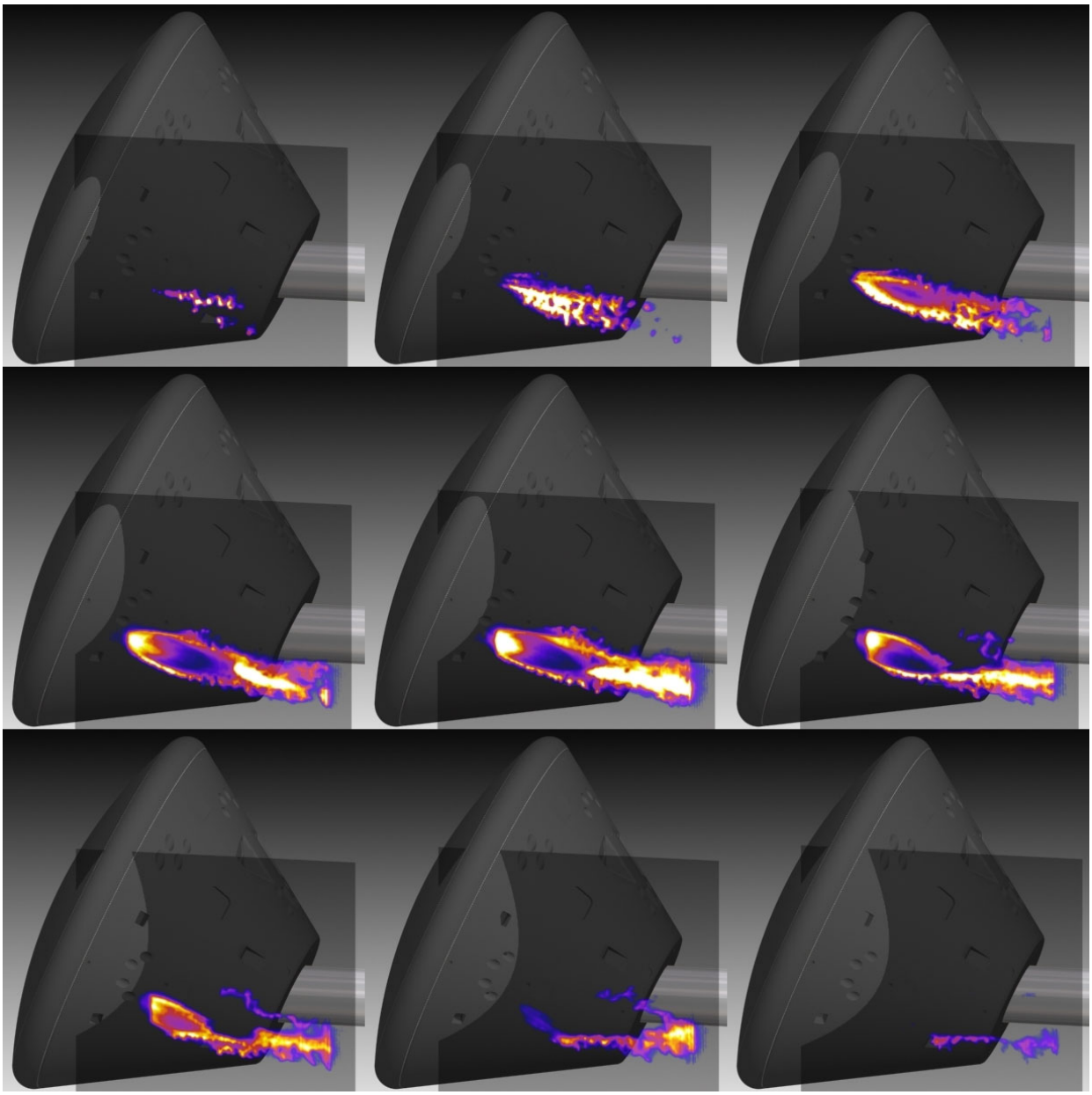

Figure 3. Scan through Orion RCS yaw jet. Run 93, Orion model (OCM-A24), P_0=8.96 MPa (1,300 psi), P_j=1.7 MPa (250 psi). Spatial resolution in the imaging plane is 4.8 pixels/mm (122 pixels/in.) vertically and 4.9 pixels/mm (123 pixels/in.) horizontally. Capsule heatshield diameter is 127 mm (5.0 in.) and sting diameter is 19 mm (0.75 in.).

In Fig. 3, a series of such single-shot images are shown from a scan of the laser sheet through an Orion RCS yaw jet. The images shown were taken at equally spaced intervals, moving away from the viewer, toward the model centerline. (Images were actually acquired with a fidelity of approximately 1 image per 0.4 mm for this run, but are shown at 34 mm intervals.) Note that the flow remains laminar in the supersonic expansion region of the jet, but quickly becomes turbulent after passing through normal or oblique shock structures. The paucity of jet fluid in the

planes nearing the edge of the model show that the external flow around the vehicle is deflecting portions of the jet that are not in the flow shadow of the capsule.

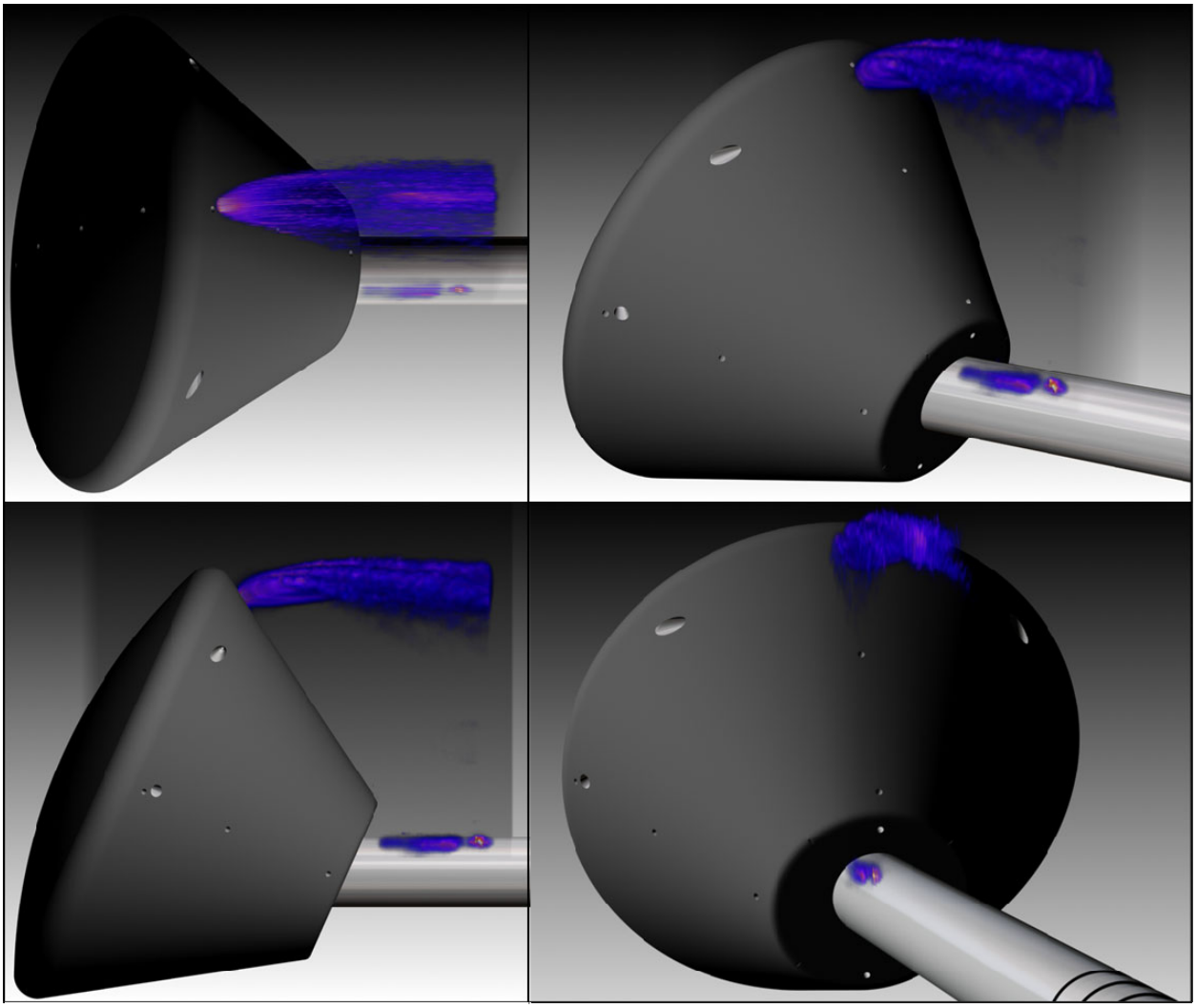

Figure 4. Volume visualization of pitch RCS jet. Images acquired during a spanwise spatial scan of the laser sheet through the flow are displayed simultaneously in a nearly-overhead view (upper left), perspective view (upper right), side view (lower left) and nearly-back view (lower right). Imaging resolution is 4.1 pixels/mm (103 pixels/in.) vertically, 4.0 pixels/mm (102 pixels/in.) horizontally, and 3.9 frames/mm (100 frames/in.) spanwise. Capsule heatshield diameter is 127 mm (5.0 in) and sting diameter is 19 mm (0.75 in.). Run 58, Apollo model (ASM-S24)

While the pitch jet seen in Figs. 1 and 2 is essentially symmetric about the model centerline, yaw and roll jets are highly three-dimensional, with no simple axis of symmetry. Volumetric measurements and post-process visualization are therefore necessary to fully characterize these type of jet structures. A better means of displaying volumetric data was explored in post-processing of this data set. In this method, all single-shot PLIF images acquired during a spatial scan are displayed simultaneously, as described in the Analysis Methods section above.

Figure 4 shows the results of this type of volume rendering for the pitch jet shown in Figs. 1 and 2. Four virtual camera views are shown: top, perspective, side, and back views.

These images provide an intuitive understanding of the spatial extent of the RCS jet flow that is difficult to glean from a single-shot image. In the top, right image of Fig. 4, an important flow feature is observed from the quasi-3D rendering that is not apparent from the single-shot images. The individual images show seemingly random unsteady transitional flow structures near the top of the jet. However, when the images are compiled into the quasi-3D volume rendering, these transitional structures line up in adjacent images, creating streamwise rope-like structures or ridges on the top of the jets. This series of streamwise ridges are perhaps once again the manifestation of a type of azimuthal cosine transitional breakdown mode.[22] In single-shot images, the flow appears unsteady and somewhat random, but the volume rendering reveals that certain features are persistent enough to form these unexpected time-averaged structures. Note that the bright spot at the base of the model is laser scatter off the sting which was not entirely blocked by the spectral filter in front of the camera. Similar camera views are shown for the yaw and roll jets in Figs. 5 and 6, respectively.

In Fig. 5, particularly from the top view, gas can be seen in the region between the main RCS jet plume and the model afterbody. The smooth appearance of this apparent line of gas is particularly interesting considering that it is a superposition of individual images that each show turbulent structures. Without the volume rendering of the data, however, the physical location of this gas stream relative to the model was difficult to determine. We postulate that this gas may be low-velocity gas from the boundary layer inside the nozzle that is subsequently entrained into the capsule wake flow. Note that while the jet is clearly being turned by the eternal flow of gas around the capsule, the jet is penetrating well beyond the shadow of the model, in contrast to the case shown in Figure 3. The location of the outer boundary of this yaw jet will provide a nice point of comparison with computed baseline (jet-off) flow streamlines around the model. The degree of deflection of the baseline shear layer provides a point of comparison as to the effectiveness of this particular nozzle configuration, compared to other nozzle geometries.

In Fig. 6, the three-dimensional structure of the roll jet is evident. As the gas exits the roll nozzle, it remains close to the model surface. This attachment of the flow to the surface was an unintended characteristic of this particular nozzle geometry. Such an interaction of an RCS jet with the surface and may have adverse effects on surface heating augmentation, particularly if the jet is created through combustion processes and has a high

stagnation temperature. Shortly after becoming detached from the surface, however, the jet flow is turned down and aft by the flow around the capsule. Again, the jet can be seen to penetrate more than one jet diameter beyond the aerodynamic shadow of the model. Note that in Fig. 6, a secondary gas stream is not observed between the primary RCS roll jet plume and the model, as was the case for the yaw jet.

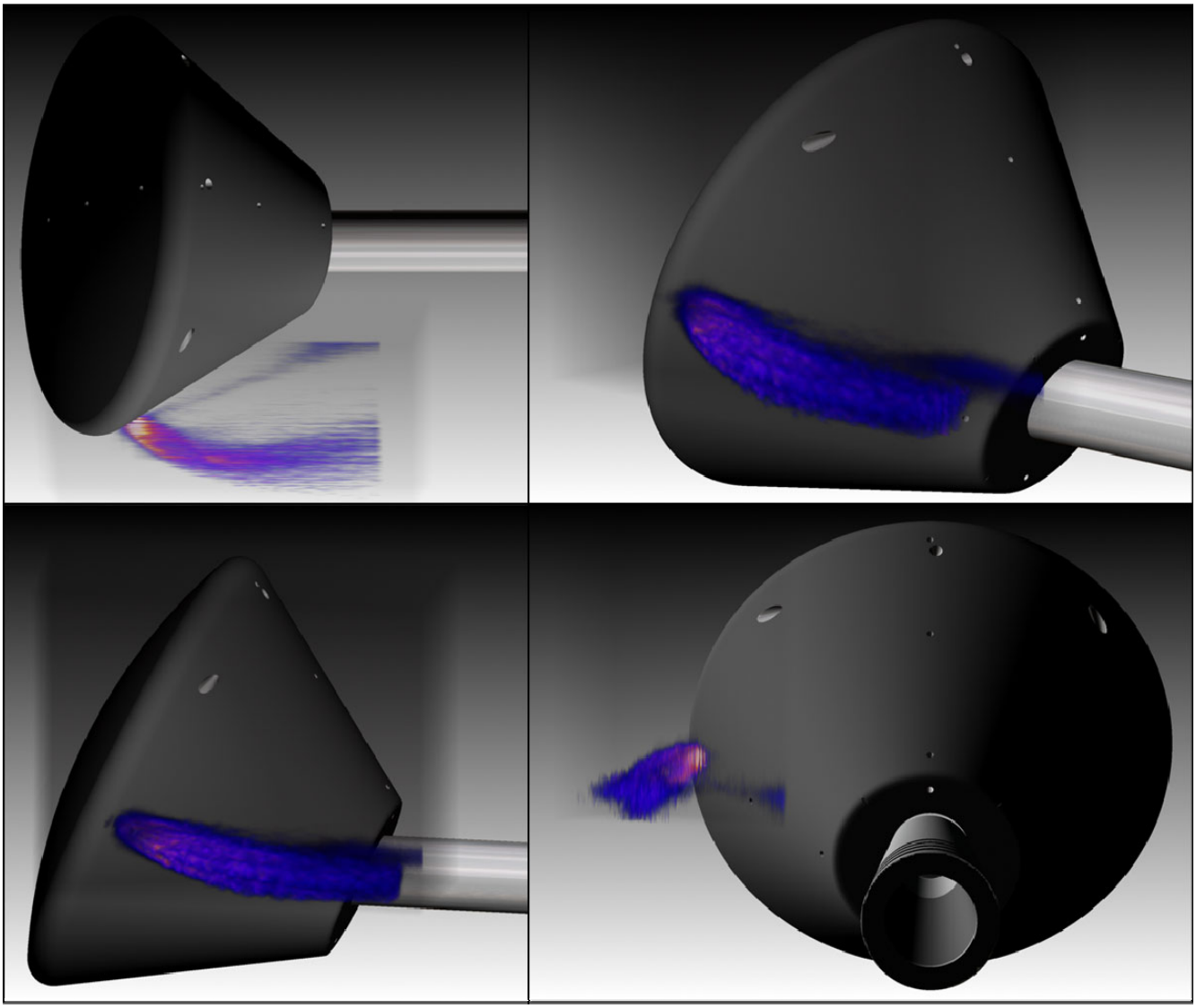

Figure 5. Volume visualization of RCS yaw jet. Imaging resolution is 4.7 pixels/mm (120 pixels/in.) vertically, 4.8 pixels/mm (121 pixels/in.) horizontally, and 3.0 frames/mm (75 frames/in.) spanwise. Capsule heatshield diameter is 127 mm (5.0 in) and sting diameter is 19 mm (0.75 in.). Run 74, Apollo model (ACM-S24).

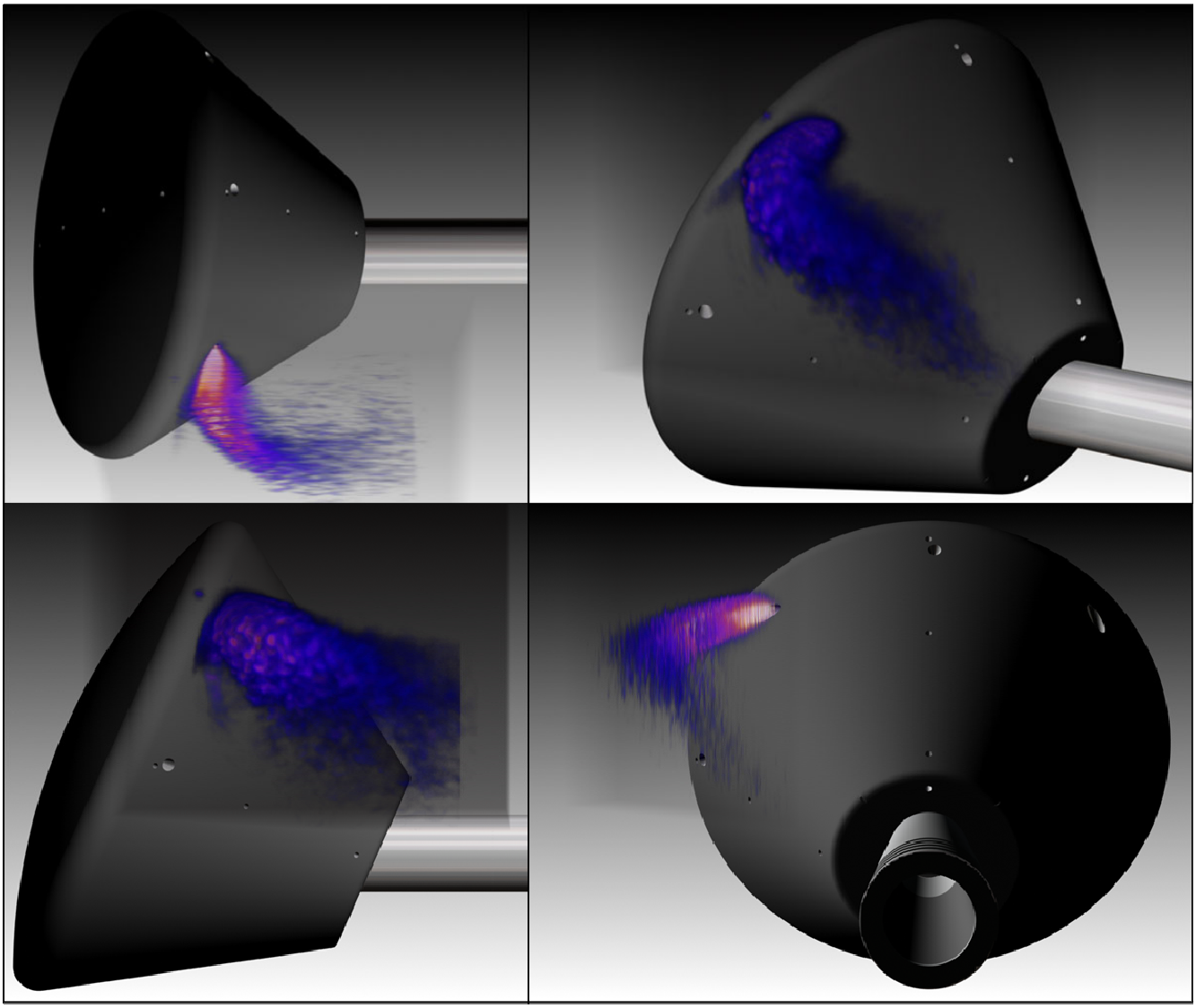

Figure 6. Volume visualization of RCS roll jet. Imaging resolution is 4.7 pixels/mm (120 pixels/in.) vertically, 4.8 pixels/mm (121 pixels/in.) horizontally, and 3.0 frames/mm (75 frames/in.) spanwise. Capsule heatshield diameter is 127 mm (5.0 in) and sting diameter is 19 mm (0.75 in.). Run 81, Apollo model.

2. Comparison of 1 vs. 4 Yaw Jets

The Orion capsule wind tunnel model (OCM-A24) was designed to allow various candidate nozzle configurations to be tested. One design option was to have up to four co-located nozzles for each pair of control jets (pitch, yaw and roll). To better understand the effect of multiple nozzles, runs were conducted with a single yaw jet activated and then with four yaw jets activated simultaneously. Visualizations from two such runs are presented in Figs. 7 and 8.

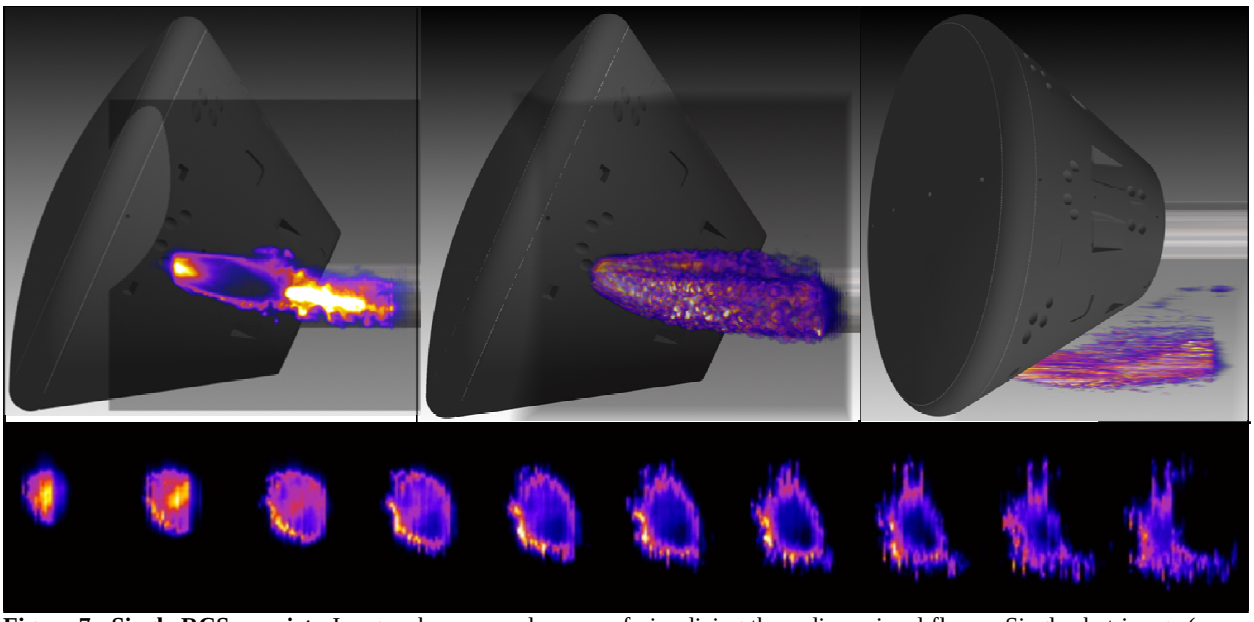

Figure 7. Single RCS yaw jet. Images show several means of visualizing three-dimensional flows. Single-shot image (upper left); side view of volume visualization (center); top view of volume visualization (upper right); and spanwise slices through the flow at 3.1 mm (0.12 in.) intervals, beginning just downstream of the nozzle exit (bottom). Capsule heatshield diameter is 127 mm (5.0 in) and sting diameter is 19 mm (0.75 in.). The slices shown here span a region covering approximately one third the width of the imaging plane. The slices have been cropped to save space, and each slice measures 33 mm (1.3 in.) high x 21 mm (0.83 in.) wide x 0.2 mm (0.008 in.) thick (in the out-of-plane direction) with an imaging resolution of 4.8 pixels/mm (123 pixels/in.) vertically, 2.4 pixels/mm (61 pixels/in.) horizontally, and 2.4 frames/mm (60 frames/in.) spanwise. Run 93, Orion model (OCM-A24).

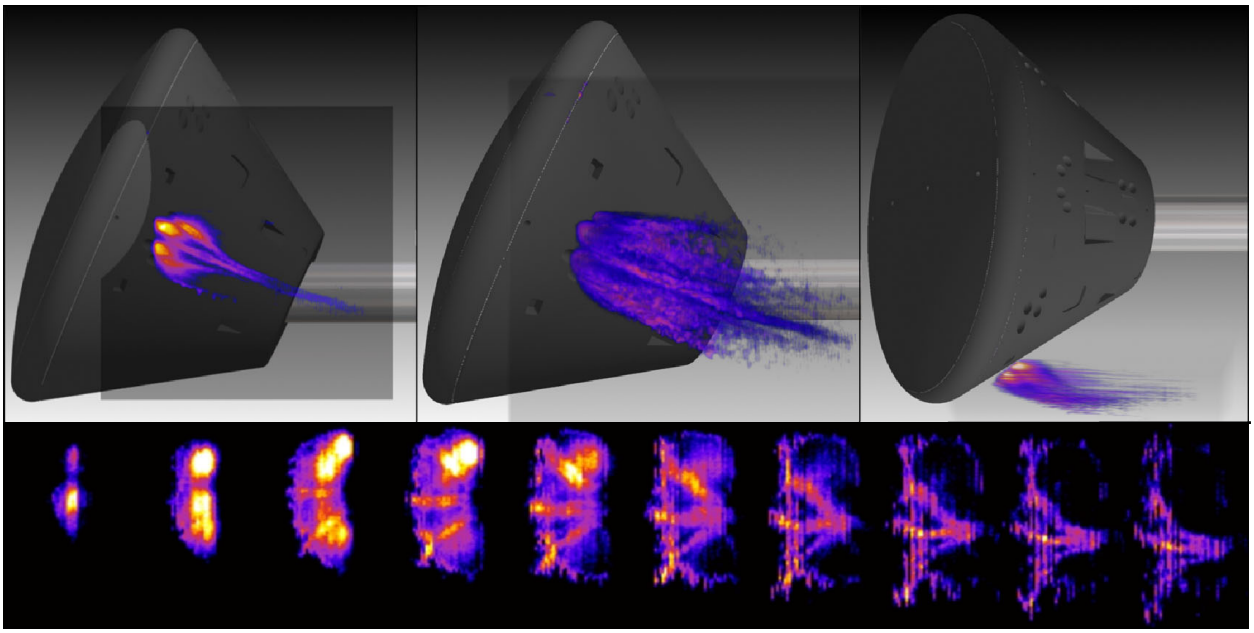

Figure 8. Four RCS yaw jets. Single-shot image (upper left); side (center) and top view of volume visualization (upper right); and spanwise slices through the flow at 3.1 mm (0.12 in.) intervals, beginning just downstream of the nozzle exits (bottom). Slices shown span a region covering about one third the width of the imaging plane, and each measures 35 mm (1.4 in.) high x 21 mm (0.83 in.) wide x 0.2 mm (0.008 in.) thick (in the out-of-plane direction) with an imaging resolution of 4.8 pixels/mm (123 pixels/in.) vertically, 2.4 pixels/mm (61 pixels/in.) horizontally, and 2.4 frames/mm (60 frames/in.) spanwise. Run 100, Orion model (OCM-A24).

In Fig. 7, the single yaw jet is seen exiting the nozzle and quickly turning downstream, pushed by the flow around the model. The single-shot image on the upper left highlights instantaneous flow structures. In the center image, volume rendering reveals the overall extent of the jet. In the top view (upper right image), turbulent traces of gas are seen to sometimes become entrained in the wake flow. Unlike the yaw jet shown for the Apollo model in Fig. 5, this yaw jet does not penetrate beyond the aerodynamic shadow of the capsule. The reconstructed cross-sectional slices shown in the bottom of Fig. 7 reveal the appearance of azimuthal modes, and in particular, the growth and bending of the outer two lobes as the jet core collapses, similar to features seen in the Apollo pitch jet in Figs. 1, 2, and 4.

The run with four activated yaw jets, shown in Fig. 8, was conducted at the same tunnel conditions and jet plenum pressure as its single-jet counterpart. The overall intensity in the images of the four jets is lower due partly to a more rapid consumption of the gas in the bottle, which resulted in an increased dilution effect. A comparison of the volume visualization top views in Fig. 8 to the corresponding images in Fig. 7 shows that the four-jet case penetrates further than the single-jet case into the flow around the capsule. The bottom image in Fig. 8 reveals interesting flow features resulting from the interaction of the four jets with the flow around the capsule as well as their interaction with each other. Note the development of three strong surfaces of interaction between the jets, becoming increasingly evident as the jet develops downstream. Also notice how the four initially round jets become distorted with distance; the outer two jets are seen to grow in diameter, whereas the inner two jets collapse and become nearly triangular in shape. The overall envelope of the combined four-jet flow does not seem to exhibit as large a degree of curvature as the single jet case shown in Fig. 7. It is also interesting to compare the cross-sectional areas of the one-jet and four-jet runs, for example the fourth cross section at the bottom of Figs. 7 and 8. Note that because the one-jet and four-jet runs both had similar jet plenum pressures and similar tunnel stagnation pressures, the effect of having four nozzles is to increase the overall nozzle exit area by a factor of four, and thus to increase the total mass flow rate by a factor of four as well. However, the combined cross-sectional area of the four jets downstream of the nozzle exits (as seen by comparing all but the first slices in Figs. 7 and 8) is roughly twice the cross-sectional area of the single jet, not four times the area as might naïvely have been expected based purely on the relative mass flow rates. Such an observation is made possible by the spatially resolved flow visualization data that PLIF can provide.

Recommendations

High fidelity three-dimensional flow visualization of the RCS jets studied in this test have revealed interacting flowfields that are characterized by a high degree of complexity. The highly three-dimensional geometry of the flows, the existence of transitional and turbulent features, and the observation of some unexpected flow phenomena (for example, the streamer of gas between the yaw jet and the capsule surface shown in Fig. 5, the azimuthal modes and resulting ridges seen for the pitch and yaw jets seen in Figs. 4, 5, and 7, or the attached flow of the roll jet seen in Fig. 6) all underscore the importance of including qualitative flow visualization along with any quantitative surface or off-body measurements in future studies of similar flows. While the test described herein was largely successful and more efficient than previous tests in the same facility, a number of improvements are suggested which should increase the range of accessible test conditions, improve the quality of the data collected, and increase the efficiency and ease of data collection and data processing.

Data collection efficiency was improved in the current experiment by minimizing the number of occasions on which dotcard images were required to be obtained. When dotcards are acquired, it is recommended that they be illuminated with an ultraviolet light source, with a wavelength as close to the NO $A \rightarrow X(0,1\text{-}5)$ fluorescence bands (237 nm – 285 nm) as possible. Using visible light to focus the camera results in a focal plane that is 1 to 2 cm further from the camera than the ultraviolet focal plane. Dotcards should be acquired coincident with any adjustments in laser sheet orientation. Additionally, it is suggested that asymmetric registration marks be added to the dotcards to eliminate potential ambiguity in the orientation of each dotcard.

One way to improve the focusing of the camera system would be to use a smaller aperture. However, this reduces the light intensity collected. In an experiment where a larger scan range is desired, reducing the aperture would allow the fluorescence to stay in focus over a much wider range as long as PLIF intensity is sufficiently high. To obtain more fluorescence, various strategies could be investigated. A higher energy laser could be used, and filters that transmit more of the fluorescence could be employed, to gain up to a factor of two more fluorescence than in the current experiment.

Conclusion

Nitric oxide PLIF has been used to study the low-density hypersonic flow of reaction control system jets into with the wake of planetary reentry capsules. Volume renderings of PLIF images acquired during sweeps of the laser sheet through the flowfield have been shown to provide valuable insight into the character and structure of flows that are highly three-dimensional. Such renderings have revealed unexpected flow features and have highlighted fine structures that were not fully anticipated. It is expected that the qualitative flow imaging results obtained in the present study will be compared with computational fluid dynamical predictions in the future. Inspection of the images showed that the placement of the RCS jets on the different configurations studied resulted in significantly different penetration distances into the oncoming flow. Also, the images indicated that azimuthal instabilties grew on the exterior boundary of the jets, leading to transition and turbulent flow downstream. Experience gained from the execution of these experiments has led to recommendations for designing follow-on experiments to be more efficient in both the design of the model and gas plumbing hardware and in the execution of the tests.

While surface measurements or off-body single-point quantitative measurements certainly provide valuable comparison data for simulations, only three-dimensional flow visualization can provide insight into the complex flow geometry and related flow structures of this type of complicated fluids problem. Perhaps the primary value of the work—and the unique information that is contained in these visualizations—is most evident when (as happens frequently) a surface or point measurement is found to deviate from a computed prediction, and both the computationalists and experimentalists want to "see what the flow is actually doing." Such a comparison may reveal, for example, that the jet trajectory, turning angle or diameter deviates significantly from what was computed. Or it may reveal the presence of turbulent structures or behavior that deviates from the anticipated level, indicating a need for higher fidelity in the turbulence modeling that is used.

In summary, three-dimensional PLIF flow visualization has been shown to be a powerful tool for temporally and spatially resolving off-body flow structures in low-density environments where no flow visualization data were previously available. These images provide valuable insight into the observed behavior of RCS jets and provide a basis for attempting to understand any discrepancies that may arise when comparing quantitative surface measurements with computational results.

Acknowledgments

We wish to acknowledge the contribution to this project from the NASA Langley Research Center 31-Inch Mach 10 Air Tunnel technicians and engineers, including Anthony Robbins, Kevin Hollingsworth, Sheila Wright, Paul Tucker, Henry "Fitz" Fitzgerald, Johnny Ellis, Stan Mason, and Doug Boggs. This work was supported by the NASA Fundamental Aeronautics Program—Hypersonics Project as well as NASA's Constellation Orion CEV Aeroscience Program (CAP). Thanks also to Richard Schwartz from ATK, Hampton Virginia, for assisting with the computer visualizations of the data.

References

[1] "NASA's Exploration Systems Architecture Study: Final Report," NASA-TM-2005-214062, November 2005.

[2] Cassel, Louis A., "Applying Jet Interaction Technology," Journal of Spacecraft and Rockets, Vol. 40, No. 4, July-August 2003.

[3] Vaughan, Chester A., "Apollo Reaction Control Systems," AIAA 68-566, *AIAA 4th Propulsion Joint Specialist Conference*, Cleveland, OH, 10-14 June 1968.

[4] Jones, Robert A., and James L. Hunt, "Effects of Cavities, Protuberances, and Reaction-Control Jets on Heat Transfer to the Apollo Command Module," NASA TM X-1063, March 1965.

[5] Danehy, Paul M., Jennifer A. Inman, Gregory J. Brauckmann, David W. Alderfer, Stephen B. Jones, and Danny P. Patry, "Visualization of a Capsule Entry Vehicle Reaction-Control System (RCS) Thruster," Journal of Spacecraft and Rockets (accepted for publication 14 March 2008; in press).

[6] Lee, M.P., B. K. McMillin, and R. K. Hanson, "Temperature Measurements in Gases Using Planar Laser-Induced Fluorescence Imaging of NO," *Applied Optics* Vol. 32, 1993, pp.5379-5396.

[7] Seitzman, J. M., F. Kychakoff, and R.K. Hanson, "Instantaneous temperature field measurements using planar laser-induced fluorescence," *Optics Letters*, Vol. 10, No. 9, Sep 1985, pp. 439-441.

[8] McMillin, B.K., J.M. Seitzman, and R.K. Hanson, "Comparison of NO and OH PLIF Temperature Measurements in a SCRAMJET Model Flowfield," AIAA 93-2035, *AIAA/SAE/ASME/ ASEE 29th Joint Propulsion Conference and Exhibit*, Monterey, CA, 28-30 June 1993.

[9] Lachney, E. R., and N. T. Clemens, "PLIF imaging of mean temperature and pressure in a supersonic bluff wake," *Experiments in Fluids*, Vol. 24, No. 4, April 1998, pp. 354-363.

[10] Fox, J.S., A.F.P. Houwing, and P.M. Danehy, "Mole-Fraction-Sensitive Imaging of Hypermixing Shear Layers," *Journal of Propulsion and Power*, Vol. 17, No. 2, March-April 2001, pp. 284-292.

[11] Paul, P.H., M.P. Lee, and R.K. Hanson, "Molecular velocity imaging of supersonic flows using pulsed planar laser-induced fluorescence of NO," *Optics Letters*, Vol. 14, No. 9, 1 May 1989, pp. 417-419.

[12] Palmer, J.L., B.K. McMillin, and R.K. Hanson, "Planar Laser-Induced Fluorescence Imaging of Underexpanded Free Jet Flow in a Shock Tunnel Facility," AIAA 91-1687, *22nd AIAA Fluid Dynamics, Plasma Dynamics and Lasers Conference*, Honolulu, HI, 24-26 June 1991.

[13] Palmer, J.L., and R.K. Hanson, "Shock tunnel flow visualization using planar laser-induced fluorescence imaging of NO and OH," *Shock Waves*, Vol. 4, 1995, pp. 313-323.

[14] Palma, P.C., *Laser-Induced Fluorescence Imaging in Free-Piston Shock Tunnels*. Ph.D. thesis, Australian National University: submitted May 1998, revised February 1999.

[15] Houwing, F., P. Danehy, P. Palma, S. O'Byrne, J. Fox, S. Mallinson, and M. Gaston, "The Application of Laser-Based Diagnostic Techniques to Supersonic and Hypersonic Flows," *2nd Australian Conference on Laser Diagnostics in Fluid Mechanics and Combustion*, Monash University, Melbourne, Australia, 9-10 December 1999.

[16] Ruyten, W. M., "Comparison of Calculated and Measured Temperature Fields in the AEDC Impulse Facility," AIAA 96-2237, *19th AIAA Advanced Measurement and Ground Testing Technology Conference*, New Orleans, LA, 17-20 June 1996.

[17] McMillan, Brian K., Jennifer L. Palmer, and Ronald K. Hanson,"Temporally resolved, two-line fluorescence imaging of NO temperature in a transverse jet in a supersonic cross flow," *Applied Optics*, Vol. 32, No. 36, 20 December 1993, pp. 7532-7545.

[18] Palma, P. C., S. G. Mallinson, S. B. O'Byrne, P. M. Danehy, and R. Hillier, "Temperature Measurements in a Hypersonic Boundary Layer Using Planar Laser-Induced Fluorescence," *AIAA Journal*, Vol. 38, No. 9, 2000, pp. 1769-1772.

[19] O'Byrne, S., P. M. Danehy, and A. F. P. Houwing, "Nonintrusive temperature and velocity measurements in a hypersonic nozzle flow, " AIAA 2002-2917, *22nd AIAA Aerodynamic Measurement Technology and Ground Testing Conference*, St. Louis, MO, 24-26 June 2002.

[20] Danehy, P.M., S. O'Byrne, A.F.P. Houwing, J.S. Fox, D.R. Smith, "Flow-Tagging Velocimetry for Hypersonic Flows Using Fluorescence of Nitric Oxide," *AIAA Journal*, Vol. 41, No. 2, Feb 2003, pp. 263-271.

[21] Danehy, P.M., A.P. Garcia, S. Borg, A.A. Dyakonov, S.A. Berry, J.A. (Wilkes) Inman, and D.W. Alderfer, "Fluorescence visualization of hypersonic flow past triangular and rectangular boundary-layer trips," AIAA 2007-0536, *45th AIAA Aerospace Sciences Meeting and Exhibit*, Reno, NV, 8-11 Jan 2007.

[22] Inman, Jennifer A. (Wilkes), Paul M. Danehy, Robert J. Nowak, and David W. Alderfer, "Identification of Instability Modes of Transition in Underexpanded Jets," AIAA 2008-4389, *38th AIAA Fluid Dynamics Conference and Exhibit*, Seattle, WA, 23-26 June 2008.

[23] Danehy, Paul M., Brett F. Bathel, Jennifer A. Inman, David W. Alderfer and Stephen B. Jones, "Stereoscopic Imaging in Hypersonic Boundary Layers using Planar Laser-Induced Fluorescence," AIAA 2008-4267, *38th AIAA Fluid Dynamics Conference and Exhibit*, Seattle, WA, 23-26 June 2008.

[24] Bathel, Brett F., Paul M. Danehy, Jennifer A. Inman, David W. Alderfer and Scott A. Berry, "PLIF Visualization of Active Control of Hypersonic Boundary Layers Using Blowing," AIAA 2008-4266, *38th AIAA Fluid Dynamics Conference and Exhibit*, Seattle, WA, 23-26 June 2008.

[25] McDaniel, J.C., Jr., C. E. Glass, D. Staack, and C. G. Miller, III, "Experimental and Computational Comparison of an Underexpanded Jet Flowfield," AIAA 2002-0305, *40th AIAA Aerospace Sciences Meeting and Exhibit*, Reno, NV, 14-17 January 2002.

[26] Watkins, A. Neal, Gregory M. Buck, Bradley D. Leighty, and William E. Lipford, "Using Pressure- and Temperature-Sensitive Paint for Global Surface Pressure and Temperature Measurements on the Aft-Body of a Capsule Reentry Vehicle," AIAA 2008-1230, *46th AIAA Aerospace Sciences Meeting and Exhibit*, Reno, NV, 7-10 January 2008.

[27] Danehy, Paul M., Jennifer A. (Wilkes) Inman, David W. Alderfer, Gregory M. Buck, and Richard J. Schwartz, "Visualization of Flowfield Modification by RCS Jets on a Capsule Entry Vehicle," AIAA 2008-1231, *46th AIAA Aerospace Sciences Meeting and Exhibit*, Reno, NV, 7-10 January 2008.

[28] Buck, Gregory M., A. Neal Watkins, Paul M. Danehy, Jennifer A. Inman, David W. Alderfer, and Artem A. Dyakonov, "Experimental Measurement of RCS Jet Interaction Effects on a Capsule Entry Vehicle," AIAA 2008-1229, *45th AIAA Aerospace Sciences Meeting and Exhibit*, Reno, NV, 7-10 January 2008.

[29] Herzberg, G., *Molecular Spectra and Molecular Structure: I. Spectra of Diatomic Molecules*, 2nd ed., with J.W.T. Spinks. Van Nostrand Reinhold Company, New York, 1950.

[30] Wilkes, Jennifer A., David W. Alderfer, Stephen B. Jones, and Paul M. Danehy, "Portable Fluorescence Imaging System for Hypersonic Flow Facilities," *JANNAF Interagency Propulsion Committee Meeting*, Colorado Springs, Colorado, 1-5 December 2003.

[31] Danehy , Paul M., David W. Alderfer , Jennifer A. Inman , Karen T. Berger , Gregory M. Buck and Richard J. Schwartz "Fluorescence Imaging and Streamline Visualization of Hypersonic Flow over Rapid Prototype Wind-Tunnel Models," Proc. IMechE, Part G: J. Aerospace Engineering, 222(G5), 2008, pp. 637-651.

[32] Micol, J.R., “Langley Aerothermodynamic Facilities Complex: Enhancements and Testing Capabilities,” AIAA 98-0147, *36th AIAA Aerospace Sciences Meeting & Exhibit*, Reno, NV, 12-15 January 1998.

[33] Schwartz, Richard J., "ViDI: Virtual Diagnostics Interface Volume 1-The Future of Wind Tunnel Testing" Contractor Report NASA/CR-2003-212667, December 2003.

[34] Autodesk 3ds Max Product Information, Autodesk Inc., http://usa.autodesk.com/adsk/servlet/index?id=5659302&siteID=123112, viewed 17 September 2008.

[35] Danehy, P. M., P. C. Palma, R. R. Boyce, A. F. P. Houwing, "Numerical simulation of laser-induced fluorescence imaging in shock-layer flows", AIAA Journal, Vol. 37, 1999, pp. 715-722.